



Известия высших учебных заведений. Прикладная нелинейная динамика. 2026. Т. 34, № 3
Izvestiya Vysshikh Uchebnykh Zavedeniy. Applied Nonlinear Dynamics. 2026;34(3)

Article

DOI: 10.18500/0869-6632-003219

**Scalable fixed-time synchronization of robotic swarms
via a novel 4D fractional-order system without equilibrium points
and with bistable dynamics**

F. Zaamoune¹✉, H. Zerimeche², R. W. Ibrahim³, A. I. Karimov⁴

¹University of Biskra, Algeria

²Constantine 1-Mentouri University, Algeria

³Al-Ayen University, Nasiriyah, Iraq

⁴St. Petersburg Electrotechnical University “LETI”, Russia

E-mail: ✉ faiza.zaamoune@univ-biskra.dz, hadjer.zerimeche@umc.edu.dz,
rabhaibrahim@yahoo.com, aikarimov@etu.ru

Received 11.03.2026, accepted 14.04.2026, available online 21.04.2026, published 29.05.2026

Abstract. Chaotic systems without equilibrium points represent a significant class of nonlinear dynamical systems because their behavior cannot be interpreted through conventional equilibrium-based analysis. *Purpose.* In this study, a novel four-dimensional fractional-order chaotic system without equilibrium points is proposed and analyzed. The *results* reveal bistable dynamics characterized by the coexistence of two distinct attractors under the same parameter set and different initial conditions, including symmetric limit cycles and chaotic attractors with different geometric structures. These dynamical features are exploited to enhance trajectory unpredictability in autonomous mobile robotic applications. Furthermore, a fixed-time synchronization framework is developed for large-scale multi-agent systems. In contrast to conventional asymptotic methods, the proposed strategy ensures convergence within a prescribed time bound independent of the initial states. The framework is then implemented in a master-slave robotic swarm, linking fractional-order reference dynamics with integer-order kinematic agents. Numerical investigations confirm the capability of the proposed method to achieve accurate synchronization and reliable trajectory tracking in networked robotic systems.

Keywords: fractional-order calculus, bistable dynamics, no-equilibrium system, fixed-time synchronization swarm robotics.

Acknowledgements. This study was supported by the Russian Science Foundation, project number 24-71-10064.

For citation: Zaamoune F, Zerimeche H, Ibrahim RW, Karimov AI. Scalable fixed-time synchronization of robotic swarms via a novel 4D fractional-order system without equilibrium points and with bistable dynamics. Izvestiya VUZ. Applied Nonlinear Dynamics. 2026;34(3):349–370. DOI: 10.18500/0869-6632-003219

This is an open access article distributed under the terms of Creative Commons Attribution License (CC-BY 4.0).

Масштабируемая синхронизация за конечное время роев роботов с помощью новой 4D-системы дробного порядка без точек равновесия и с бистабильной динамикой

Ф. Заамун¹, Х. Зеримеш², Р. В. Ибрахим³, А. И. Каримов⁴

¹Университет Мохамеда Хидера в Бискре, Алжир

²Университет братьев Ментури Константина 1, Алжир

³Университет Аль-Айн, Насирия, Ирак

⁴Санкт-Петербургский государственный электротехнический университет «ЛЭТИ» имени В. И. Ульянова (Ленина), Россия

E-mail: ✉ faiza.zaamoune@univ-biskra.dz, hadjer.zerimeche@umc.edu.dz, rabhaibrahim@yahoo.com, aikarimov@etu.ru

Поступила в редакцию 11.03.2026, принята к публикации 14.04.2026,
опубликована онлайн 21.04.2026, опубликована 29.05.2026

Аннотация. Хаотические системы без точек равновесия представляют собой важный класс нелинейных динамических систем, поскольку их поведение невозможно интерпретировать с помощью обычного анализа, основанного на равновесии. *Цель.* В этом исследовании предложена и проанализирована новая четырёхмерная хаотическая система дробного порядка без точек равновесия. *Результаты* показывают бистабильную динамику, характеризующуюся сосуществованием двух различных аттракторов при одном и том же наборе параметров и при различных начальных условиях, включая симметричные предельные циклы и хаотические аттракторы с различной геометрической структурой. Эти динамические особенности используются для повышения непредсказуемости траекторий в автономных мобильных роботизированных приложениях. Кроме того, для крупномасштабных мультиагентных систем разработана система синхронизации с фиксированным временем. В отличие от традиционных асимптотических методов, предлагаемая стратегия обеспечивает сходимость в течение заданного времени независимо от начальных условий. Затем фреймворк реализуется в роботизированном рое «ведущий–ведомый», связывая эталонную динамику дробного порядка с кинематическими агентами, описываемыми системами целого порядка. Численные исследования подтверждают способность предложенного метода достигать точной синхронизации и надёжного отслеживания траектории в сетевых роботизированных системах.

Ключевые слова: дробный математический анализ, бистабильная динамика, неравновесная система, роевая робототехника с синхронизацией за конечное время.

Благодарности. Исследование выполнено при поддержке Российского научного фонда, проект № 24-71-10064.

Для цитирования: Zaamoune F., Zerimeche H., Ibrahim R. W., Karimov A. I. Scalable fixed-time synchronization of robotic swarms via a novel 4D fractional-order system without equilibrium points and with bistable dynamics [Заамун Ф., Зеримеш Х., Ибрахим Р. В., Каримов А. И. Масштабируемая синхронизация за конечное время роев роботов с помощью новой 4D-системы дробного порядка без точек равновесия и с бистабильной динамикой] // Известия вузов. ПНД. 2026. Т. 34, № 3. С. 349–370. DOI: 10.18500/0869-6632-003219. EDN: XEKTRW

Статья опубликована на условиях Creative Commons Attribution License (CC-BY 4.0).

Introduction

The use of chaotic dynamics in engineering has evolved considerably since Lorenz first revealed the sensitive dependence of nonlinear systems on initial conditions [1]. Beyond its theoretical significance, chaos has become an important tool in secure communication systems [2,3] and autonomous engineering applications [4,5]. Classical chaotic oscillators, such as the Rössler [6], Chen [7], and Sprott [8] systems, have been extensively studied; however, these models generally possess unstable equilibrium points, from which phase-space reconstruction may be facilitated. For this reason, increasing attention has recently

been directed toward non-equilibrium chaotic systems, especially those without equilibrium points or with dynamics that cannot be fully interpreted through conventional equilibrium-based analysis [9–12]. Owing to their increased complexity and resistance to analytical reconstruction, such systems are regarded as promising candidates for secure and advanced engineering applications [13–15].

Fractional calculus provides an effective framework for describing memory and hereditary effects in complex physical systems [16, 17]. In comparison with integer-order models, fractional-order chaotic systems are often characterized by richer and more diverse dynamical behaviors [18–20]. Significant efforts have therefore been devoted to the study of fractional extensions of well-known chaotic systems [21–23]. Recent investigations have further demonstrated that four-dimensional fractional-order models may exhibit hyperchaotic regimes, toroidal responses, and coexistence phenomena of considerable practical interest, particularly in applications related to encryption, nonlinear control, and complex-signal generation [24–27].

In multi-agent systems, synchronization constitutes the fundamental mechanism through which coordinated collective behavior can be achieved [28, 29]. Although asymptotic and exponential synchronization methods have been widely used and have proved effective in many settings [30–32], their convergence either requires theoretically infinite time or remains dependent on the initial conditions. Such a limitation becomes critical in time-sensitive and mission-critical applications, including secure robotic swarms. To overcome this drawback, fixed-time synchronization has emerged as a more suitable alternative [33–35]. By means of Lyapunov-based design techniques, fixed-time strategies ensure convergence within a prescribed upper bound T_{\max} that is independent of the initial states [36–38]. This property makes such methods especially attractive for practical deployment in complex dynamic networks [39–41].

The integration of chaotic dynamics into mobile robotics has also attracted considerable attention [42, 43]. Chaotic trajectories, owing to their topological transitivity and strong unpredictability, can enhance workspace exploration and coverage, which is advantageous in patrol, surveillance, and search-and-rescue operations [44–46]. In addition, fractional-order kinematic models offer extra flexibility by incorporating nonlocal dynamical effects into the robot motion description [47–49]. Nevertheless, the synchronization of large-scale robotic swarms under chaotic reference dynamics remains a challenging problem [50–52]. Effective control laws must therefore be developed to preserve coordinated motion in the presence of nonlinear dynamics, model uncertainty, and external disturbances [53, 54].

In this work, a novel four-dimensional fractional-order chaotic system is proposed and is characterized by the complete absence of equilibrium points. The obtained results reveal bistable dynamics, where two distinct attractors coexist under identical parameter values and different initial conditions. To explore its practical relevance, fixed-time synchronization between the fractional-order and integer-order forms of the system is investigated. Through this framework, convergence is guaranteed within a prescribed time bound independent of the initial states, thereby establishing a robust link between fractional-order and integer-order dynamics for control and communication purposes. The resulting chaotic behavior is then exploited in the trajectory generation of a differential-drive mobile robot, through which flexible and adaptive motion planning is achieved. In addition, the developed synchronization framework is shown to preserve its effectiveness as the number of agents increases, which makes it suitable for real-time and mission-critical multi-robot applications. Accordingly, both theoretical contributions to nonlinear chaotic-system analysis and practical advantages for robotic applications are provided.

The remainder of this paper is organized as follows. Section 2 summarizes the basic concepts of fractional calculus. Section 3 presents the mathematical model of the proposed four-dimensional fractional-order chaotic system together with its main dynamical behaviors. Section 4 is devoted to the fixed-time synchronization analysis. Section 5 discusses the application to wireless mobile robots. Finally, Section 6 concludes the paper.

1. Fractional derivative and basic definitions

This study utilizes the Caputo definition of the different definitions of fractional integrals and derivatives. According to Ref. [55, 56], the definitions of the Caputo fractional integral and derivative are given as follows:

Definition 1. The fractional integral of a function $f(t)$ of order $q > 0$ is defined by

$$I^q f(t) = \frac{1}{\Gamma(q)} \int_{t_0}^t (t - \tau)^{q-1} f(\tau) d\tau,$$

where $t \geq t_0$, and $\Gamma(q)$ denotes the Gamma function, which is given by

$$\Gamma(s) = \int_0^\infty t^{s-1} e^{-t} dt.$$

Definition 2. According to Caputo's definition, the fractional derivative of order $q > 0$ of a function $f(t) \in C^n([t_0, +\infty), \mathbb{R})$, where $n \in \mathbb{N}$ is such that $n - 1 \leq q < n$, is defined as

$$D^q f(t) = \frac{1}{\Gamma(n - q)} \int_{t_0}^t \frac{f^{(n)}(s)}{(t - s)^{q-n+1}} ds.$$

In particular, when $0 < q < 1$, the Caputo fractional derivative becomes

$$D^q f(t) = \frac{1}{\Gamma(1 - q)} \int_{t_0}^t \frac{f'(s)}{(t - s)^q} ds.$$

Definition 3. The Laplace transform of the Caputo fractional derivative is expressed as

$$\mathcal{L} \{ {}^C D_t^\alpha f(t) \} = s^\alpha F(s) - \sum_{k=0}^{n-1} s^{\alpha-k-1} f^{(k)}(0), \quad (\alpha > 0, n - 1 < \alpha \leq n). \quad (1)$$

In particular, for $\alpha \in (0, 1]$, the expression simplifies to:

$$\mathcal{L} \{ {}^C D_t^\alpha f(t) \} = s^\alpha F(s) - s^{\alpha-1} f(0). \quad (2)$$

The Laplace transform of the Riemann Liouville fractional integral is:

$$\mathcal{L} \{ J^\alpha f(t) \} = s^{-\alpha} F(s), \quad (\alpha > 0). \quad (3)$$

2. Mathematical model

A new four-dimensional autonomous nonlinear system is formulated in the fractional-order domain. The proposed structure contains coupled bilinear terms, a quartic nonlinear term, and an absolute-value nonlinearity, whose interaction gives rise to complex dynamical behaviors. The mathematical model is formulated as

$$\begin{cases} D^{q_1} x_1(t) = x_2(t), \\ D^{q_2} x_2(t) = -x_3(t)x_2(t) - x_1(t) - a_1 x_4(t), \\ D^{q_3} x_3(t) = a_2 x_2^4(t) - a_3 |x_2(t)| - a_5, \\ D^{q_4} x_4(t) = -a_4 x_4(t) + x_2(t)x_3(t), \end{cases} \quad (4)$$

where $x_1(t)$, $x_2(t)$, $x_3(t)$, and $x_4(t)$ denote the state variables of the proposed system, while a_1 , a_2 , a_3 , a_4 , and a_5 are positive constant parameters. The quantities $q_i \in (0, 1]$, $i = 1, \dots, 4$, represent the fractional orders of the corresponding state equations.

To determine the equilibrium points of system (4), the following algebraic system must be solved:

$$x_2(t) = 0, \quad (5a)$$

$$-x_3(t)x_2(t) - x_1(t) - a_1x_4(t) = 0, \quad (5b)$$

$$a_2x_2^4(t) - a_3|x_2(t)| - a_5 = 0, \quad (5c)$$

$$-a_4x_4(t) + x_2(t)x_3(t) = 0. \quad (5d)$$

From (5a), the condition $x_2 = 0$ is obtained. Upon substitution of $x_2 = 0$ into (5c), the relation $-a_5 = 0$ is derived, which leads to a contradiction because a_5 is a positive constant. It is therefore concluded that system (4) admits no equilibrium points.

In the following sections, the dynamical behavior of system (4) is examined separately for the integer-order and fractional-order cases.

2.1. Integer-order case. To comprehensively investigate the dynamical characteristics of the proposed model in the integer-order domain, the derivative orders are set to $q_i = 1$ for $i = 1, \dots, 4$. The system's behavior is analyzed by varying the bifurcation parameter a_3 across the interval $[0, 2]$, while the remaining system parameters are held constant at $a_1 = 0.5$, $a_2 = 0.9$, $a_4 = 5.5$, and $a_5 = 1.6$. For the numerical simulations, the initial condition is chosen as $x_0 = (0.2, 0.3, 0.1, 0.5)$. Under these configurations, the integer-order form of system (4) exhibits rich chaotic dynamics, as visually confirmed by the phase portraits in Fig. 1. To rigorously validate the presence of chaos, the Lyapunov exponent spectrum a fundamental diagnostic tool that quantifies the average exponential divergence of nearby trajectories is computed [57]. The evolution of the Lyapunov exponents with respect to a_3 is depicted in Fig. 2, *a*. Notably, the computed spectrum accurately captures a strictly zero Lyapunov exponent ($L_2 = 0$), which perfectly aligns with the theoretical properties of an autonomous continuous-time

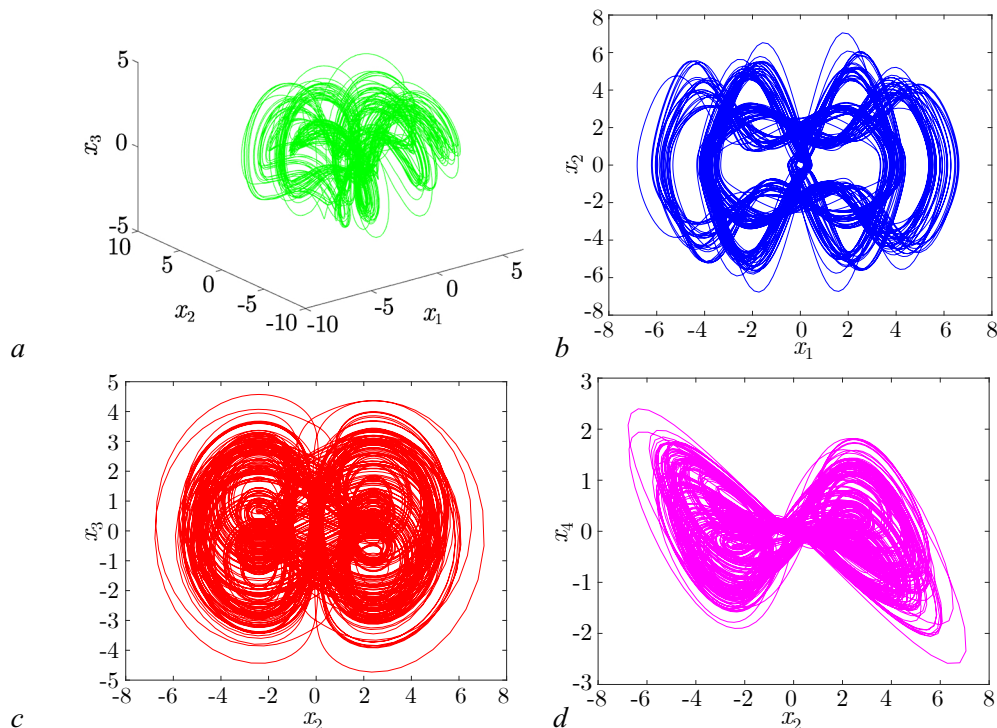


Fig. 1. Phase portraits of integer-order nonlinear system (4) for $a_1 = 0.5$, $a_2 = 0.9$, $a_3 = 1.5$, $a_4 = 5.5$, and $a_5 = 1.6$, and $q_1 = q_2 = q_3 = q_4 = 1$ with the initial condition $(0.2, 0.3, 0.1, 0.5)$. *a* – $(x_1 - x_2 - x_3)$ plane; *b* – $(x_1 - x_2)$ plane; *c* – $(x_2 - x_3)$ plane; *d* – $(x_2 - x_4)$ plane (color online)

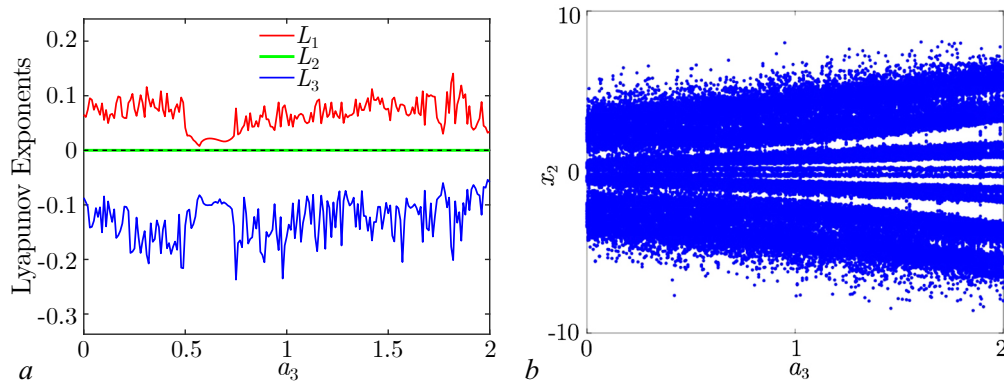


Fig. 2. The Lyapunov exponent spectrum and the bifurcation diagram with respect to the parameter $a_3 \in [0, 2]$ for $a_1 = 0.5$, $a_2 = 0.9$, $a_4 = 5.5$, and $a_5 = 1.6$, $q_1 = q_2 = q_3 = q_4 = 1$ and the initial condition $(0.2, 0.3, 0.1, 0.5)$. *a* – The enlarged fragment of the Lyapunov exponent spectrum displaying the three dominant exponents (L_1 , L_2 , and L_3); *b* – the corresponding bifurcation diagram (color online)

dynamical system. Furthermore, the corresponding bifurcation diagram over $a_3 \in [0, 2]$ is presented in Fig. 2, *b*, demonstrating a strong consistency with the calculated Lyapunov spectrum and clearly revealing the parameter regions where chaotic and periodic behaviors emerge.

2.2. Fractional-order case. The chaotic behavior of system (4) in the fractional-order domain is initially investigated by assigning a uniform fractional order $q_i = 0.985$ to all state variables, with the parameters fixed at $a_1 = 0.5$, $a_2 = 0.9$, $a_3 = 1.5$, $a_4 = 5.5$, and $a_5 = 1.6$. Under these specific settings, the system exhibits a complex chaotic attractor, as clearly illustrated by the 3D and 2D phase portraits in Fig. 3.

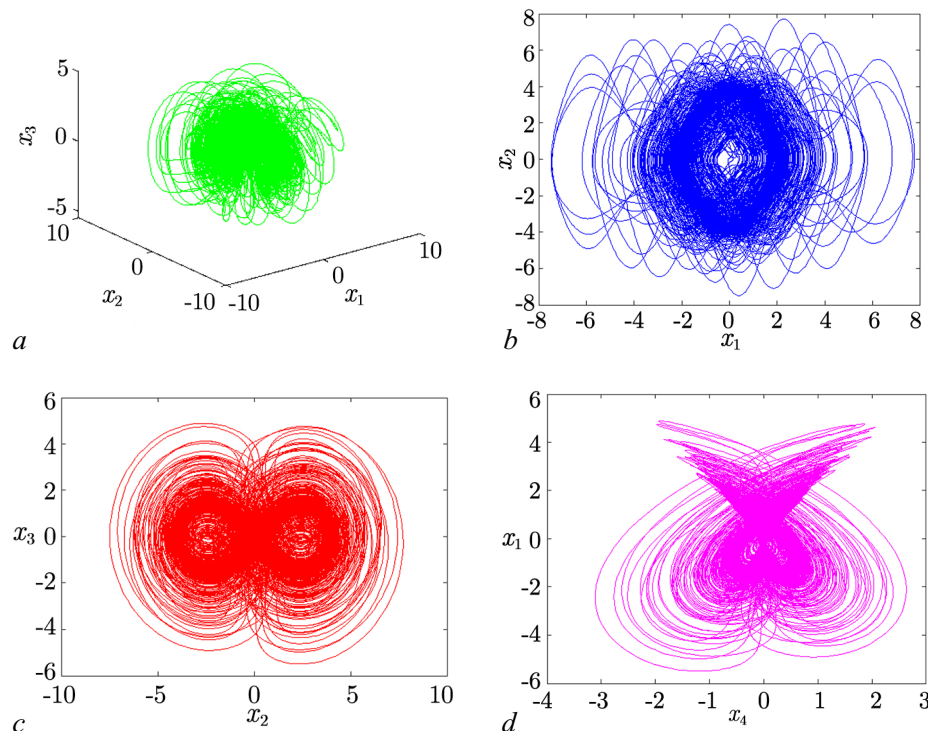


Fig. 3. Phase portraits of fractional-order system (4) for $a_1 = 0.5$, $a_2 = 0.9$, $a_3 = 1.5$, $a_4 = 5.5$, and $a_5 = 1.6$, $q_1 = q_2 = q_3 = q_4 = 0.985$ with the initial condition $(0.2, 0.3, 0.1, 0.5)$. *a* – $(x_1 - x_2 - x_3)$ plane; *b* – $(x_1 - x_2)$ plane; *c* – $(x_1 - x_3)$ plane; *d* – $(x_2 - x_4)$ plane (color online)

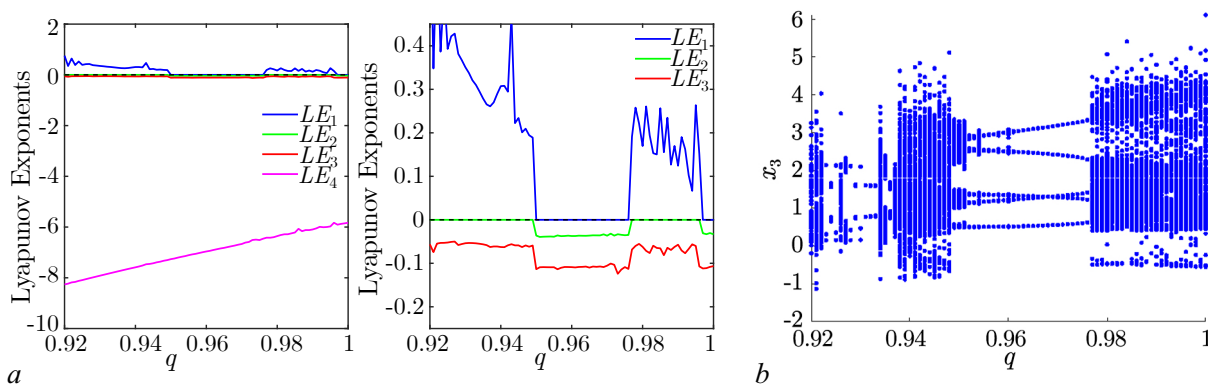


Fig. 4. The Lyapunov exponent spectrum and the bifurcation diagrams with respect to the parameter $q \in [0.92, 1]$ for $a_1 = 0.5$, $a_2 = 0.9$, $a_3 = 1.5$, $a_4 = 5.5$, and $a_5 = 1.6$, $q_1 = q_2 = q_3 = q_4 = 0.985$ and the initial condition $(0.2, 0.3, 0.1, 0.5)$. *a* – The Lyapunov exponent spectrum shown in two panels: the full spectrum including the highly negative LE_4 (left), and an enlarged fragment detailing the three dominant exponents (LE_1 , LE_2 , and LE_3) that strictly mirrors the dynamic transitions without any numerical oscillations (right); *b* – the corresponding bifurcation diagram (color online)

To rigorously validate the presence of this chaotic behavior and analyze the divergence of neighboring trajectories, the Lyapunov exponent spectrum is computed utilizing a highly refined algorithm based on the analytical Jacobian matrix [39,40]. As shown in Fig. 4, *a*, the results confirm the presence of chaos in specific regions through the existence of a positive maximum Lyapunov exponent ($LE_1 > 0$), accompanied by a strictly zero second exponent ($LE_2 = 0$). This perfectly flat and stable zero line aligns exactly with the theoretical expectations of a continuous-time autonomous system, completely eliminating any previous numerical oscillation artifacts.

In addition, a comprehensive bifurcation analysis is carried out to examine the qualitative changes in the system dynamics as the fractional order q is varied over the interval $[0.92, 1]$. For this purpose, system (4) is numerically integrated by means of the Adams–Bashforth–Moulton method [58]. The resulting bifurcation diagram, illustrated in Fig. 4, *b*, provides a clear visual description of the dynamical regimes exhibited by the system. Most importantly, a direct comparison between the Lyapunov spectrum and the bifurcation diagram reveals a strict and perfect correspondence. When the system enters the periodicity windows (e.g., the stable limit cycles clearly visible between $q = 0.950$ and $q = 0.976$), the maximum Lyapunov exponent (LE_1) drops sharply and strictly to zero, while the remaining exponents become strictly negative. This flawless correlation validates the consistency between the dynamically computed Lyapunov exponents and the observed periodic behaviors associated with the fractional-order operator.

2.3. Characterization of hidden bistability. Hidden bistability is demonstrated in the proposed system despite the complete absence of equilibrium points. This phenomenon is confirmed through bifurcation analysis and phase-space reconstruction. Numerical simulations reveal that two distinct attractors can be obtained under identical parameter values when the initial condition is varied in the form $(x_1(0), 0.2, 0.3, 0.2)$ over the fractional-order range $q \in [0.9, 1]$. The observed bistable behavior provides a clear explanation for the periodic windows appearing in the bifurcation diagrams that are not always reflected in the Lyapunov exponent spectrum. In such non-equilibrium models, the asymptotic response is determined by the corresponding basin of attraction; therefore, a single-path Lyapunov exponent computation may follow a chaotic branch while a coexisting periodic branch remains simultaneously present.

First, symmetric limit cycles with nontrivial periodicity and broken rotational symmetry are obtained for $a_1 = 0.5$, $a_2 = 0.8$, $a_3 = 1.5$, $a_4 = 5.5$, and $a_5 = 1.6$. As shown in Fig. 5, *a*, the green attractor is generated from the initial condition $x_1(0) = 2.5$, whereas the red attractor is generated

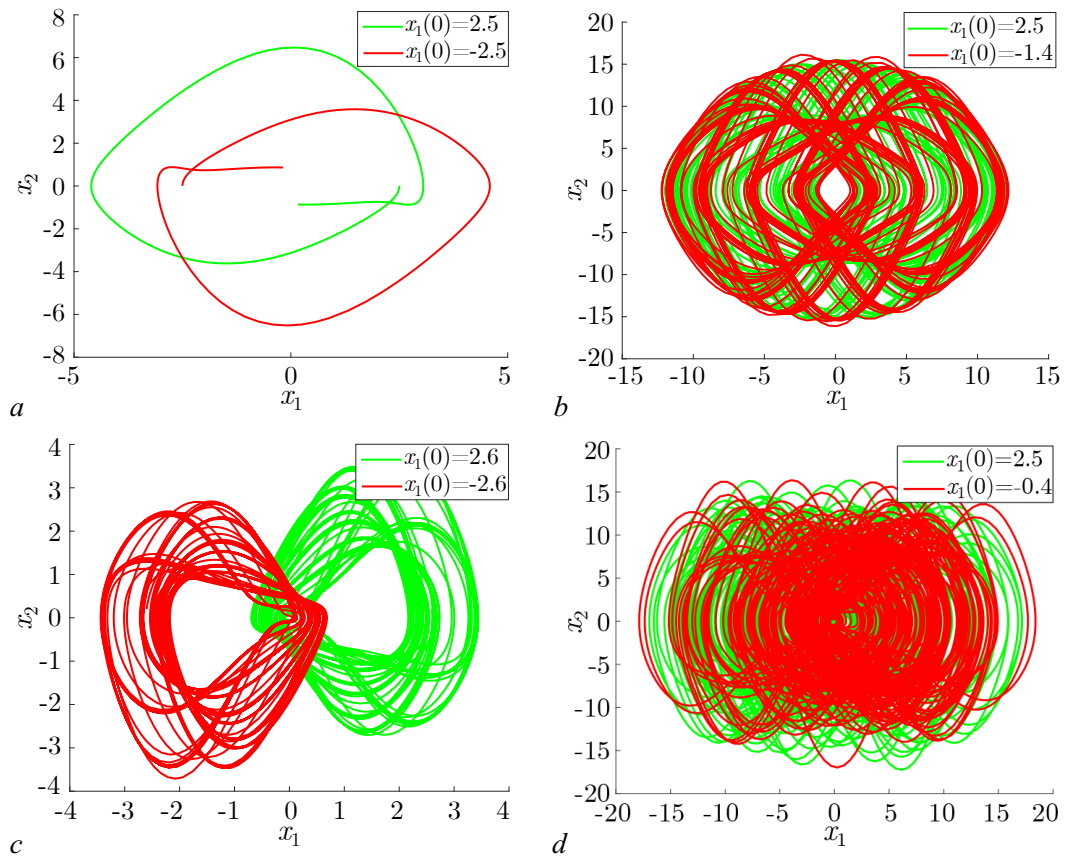


Fig. 5. Bistable coexisting attractors of system (4) obtained from the initial conditions $(x_1(0), 0.2, 0.3, 0.2)$ for $q \in [0.9, 1]$: *a* – symmetric limit cycles for $a_1 = 0.5$ and $a_5 = 1.6$; *b* – bistable chaotic attractors with different amplitudes for $a_1 = 0.1$ and $a_5 = 0.8$; *c* – symmetric bistable chaotic attractors for $a_1 = 2.5$ and $a_5 = 0.6$; *d* – two distinct bistable chaotic attractors for $a_1 = 2.5$ and $a_5 = 0.6$ (color online)

from $x_1(0) = -2.5$. Second, for $a_1 = 0.1$, $a_2 = 0.1$, $a_3 = 0.5$, $a_4 = 0.2$, and $a_5 = 0.8$, bistable chaotic behavior with different amplitudes is observed. In this case, the green attractor is obtained from $x_1(0) = 2.5$, whereas the red attractor is obtained from $x_1(0) = -1.4$, as illustrated in Fig. 5, *b*.

Moreover, a symmetric bistable pattern is identified for $a_1 = 2.5$, $a_2 = 0.9$, $a_3 = 0.5$, $a_4 = 5.5$, and $a_5 = 0.6$. The corresponding attractors are produced from the initial conditions $x_1(0) = 2.6$ for the green trajectory and $x_1(0) = -2.6$ for the red trajectory, as depicted in Fig. 5, *c*. Finally, another bistable chaotic regime is observed for the same parameter set, where two distinct chaotic attractors are generated from $x_1(0) = 2.5$ and $x_1(0) = -0.4$, respectively, as shown in Fig. 5, *d*. These results demonstrate that, under the same system parameters, different long-term dynamical behaviors can be selected solely through the initial conditions. Such persistent bistable oscillatory responses indicate strong potential for applications requiring enhanced unpredictability and flexible state selection, particularly in secure communication and nonlinear control systems.

3. Fixed-time synchronization

This study presents a novel fixed-time synchronization method for the new chaotic system (4) in both its integer-order and fractional-order representations. The following lemma and theorem are presented:

Lemma 1. [59] Let $z_1, z_2, \dots, z_n > 0$, $0 < l \leq 1$, and $r > 1$. Then, the following two inequalities hold:

$$\sum_{i=1}^n z_i^l \geq \left(\sum_{i=1}^n z_i \right)^l,$$

$$\sum_{i=1}^n z_i^r \geq n^{1-r} \left(\sum_{i=1}^n z_i \right)^r.$$

The following fixed-time stability result is adopted from [41].

Theorem 1. Consider the fractional-order system

$${}_{t_0}D_t^q x(t) = f(t, x(t)).$$

The origin is said to be fixed-time stable if there exists a positive definite Lyapunov function $V(t, x(t))$, denoted for simplicity by $V(t)$, such that

$${}^0D_t^\alpha V(t) \leq \frac{\lambda_1 \Gamma(1-\gamma)}{\Gamma(2-\alpha)\Gamma(\alpha-\gamma+1)} V^{1-\alpha+\gamma}(t) - \frac{\lambda_2 \Gamma(1-\beta)}{\Gamma(2-\alpha)\Gamma(\alpha-\beta+1)} V^{1-\alpha+\beta}(t), \quad (6)$$

where $\lambda_1 > 0$, $\lambda_2 > 0$, $1 < \gamma < \alpha + 1$, and $\alpha - 1 < \beta < \alpha$. Then, the origin of the considered system is fixed-time stable for any initial condition, and the corresponding settling time is estimated by

$$T = \left(\frac{\Gamma(1+\alpha)}{\lambda_1} \right)^{\frac{1}{\alpha}} + \left(\frac{\Gamma(1+\alpha)}{\lambda_2} \right)^{\frac{1}{\alpha}}.$$

Consider the following integer-order new chaotic system as the drive system:

$$\begin{cases} \dot{x}_1(t) = x_2(t), \\ \dot{x}_2(t) = -x_3(t)x_2(t) - x_1(t) - a_1x_4(t), \\ \dot{x}_3(t) = a_2x_2(t)^4 - a_3|x_2(t)| - a_5, \\ \dot{x}_4(t) = -a_4x_4(t) + x_2(t)x_3(t), \end{cases} \quad (7)$$

Let the following fractional-order new chaotic system be the response system:

$$\begin{cases} D^q y_1(t) = y_2(t) + u_1, \\ D^q y_2(t) = -y_3(t)y_2(t) - y_1(t) - a_1y_4(t) + u_2, \\ D^q y_3(t) = a_2y_2(t)^4 - a_3|y_2(t)| - a_5 + u_3, \\ D^q y_4(t) = -a_4y_4(t) + y_2(t)y_3(t) + u_4, \end{cases} \quad (8)$$

Where $S : \mathbb{R}^n \rightarrow \mathbb{R}^n$ and $W : \mathbb{R}^n \rightarrow \mathbb{R}^n$ are two continuous differentiable functions.

$$e(t) = S(x) - W(y). \quad (9)$$

The fixed gains in (11) are extended to the adaptive form:

$$\begin{aligned}\lambda_1(t) &= 0.5 + 2e^{-0.1\|e(t)\|}, \\ \gamma(t) &= 0.9 - 0.2 \cos(2\pi t/10).\end{aligned}\tag{13}$$

Theorem 2. *The adaptive controller preserves fixed-time stability provided that $\frac{d\lambda_1}{dt} < 0$ and $\gamma(t) \in [0.7, 1.1]$.*

$$\begin{aligned}\text{where } 0 < \gamma_i < 1, \quad \lambda_1 > 0, \quad \lambda_2 &= -\frac{4^{\frac{\gamma_1}{2}} \Gamma(2-q) \Gamma\left(\frac{3-\gamma_1}{2}\right)}{\Gamma\left(\frac{3-\gamma_1}{2}-q\right)}, \quad \lambda_3 = -\frac{4^{\frac{\gamma_1}{2}} \Gamma(2-q) \Gamma\left(\frac{3-\gamma_1}{2}\right)}{\Gamma\left(\frac{3-\gamma_1}{2}-q\right)}, \\ \lambda_4 &= \lambda_2 - \frac{4^{\frac{\gamma_1}{2}} \Gamma(2-q) \Gamma\left(\frac{3-\gamma_1}{2}\right)}{\Gamma\left(\frac{3-\gamma_1}{2}-q\right)}.\end{aligned}$$

Theorem 3. *The drive system (7) achieves fixed-time synchronization with the response (8) when the control input is defined by (11).*

Proof 1. *By following the methodology presented in [60], and by substituting the control law defined in equations (11)–(12) into the slave system given in equation (8), the following reformulated slave system is obtained:*

$$\begin{cases} D^q y_1(t) = J^{1-q_1} (y_2(t) - r_1(t)), \\ D^q y_2(t) = J^{1-q_2} (-y_3(t)y_2(t) - y_1(t) - a_1 y_4(t) - r_2(t)), \\ D^q y_3(t) = J^{1-q_3} (a_2 y_2(t)^4 - a_3 |y_2(t)| - a_5 - r_3(t)), \\ D^q y_4(t) = J^{1-q_4} (-a_4 y_4(t) + y_2(t)y_3(t) - r_4(t)). \end{cases}\tag{14}$$

By applying the Laplace transform to equation (14) and denoting $F(s) = \mathcal{L}(Y(t))$, the following expression is obtained:

$$\begin{cases} s^p F(s) - s^{p-1} y_1(0) = s^{p-1} \mathcal{L}(y_2(t) - r_1(t)), \\ s^p F(s) - s^{p-1} y_2(0) = s^{p-1} \mathcal{L}(-y_3(t)y_2(t) - y_1(t) - a_1 y_4(t) - r_2(t)), \\ s^p F(s) - s^{p-1} y_3(0) = s^{p-1} \mathcal{L}(a_2 y_2(t)^4 - a_3 |y_2(t)| - a_5 - r_3(t)), \\ s^p F(s) - s^{p-1} y_4(0) = s^{p-1} \mathcal{L}(-a_4 y_4(t) + y_2(t)y_3(t) - r_4(t)). \end{cases}\tag{15}$$

By multiplying both sides of equation (15) by s^{1-p} and then applying the inverse Laplace transform, a new expression for the slave system is obtained:

$$\begin{cases} \dot{y}_1(t) = y_2(t) - r_1(t), \\ \dot{y}_2(t) = -y_3(t)y_2(t) - y_1(t) - a_1 y_4(t) - r_2(t), \\ \dot{y}_3(t) = a_2 y_2(t)^4 - a_3 |y_2(t)| - a_5 - r_3(t), \\ \dot{y}_4(t) = -a_4 y_4(t) + y_2(t)y_3(t) - r_4(t), \end{cases}\tag{16}$$

Then, the error system is obtained as

$$\begin{aligned} \dot{e}_i(t) = & -\lambda_1 e_i(t) - \lambda_2 \operatorname{sign}(e_i(t)) |e_i(t)|^{1+\gamma_1} - \\ & - \lambda_3 \operatorname{sign}(e_i(t)) |e_i(t)|^{1-\gamma_1} - \lambda_4 \operatorname{sign}(e_i(t)) |e_i(t)|^{1+\gamma_1}, \end{aligned} \quad (17)$$

where $i = (1, \dots, 4)$. Now, construct the following Lyapunov function:

$$V(t) = \frac{1}{2} \left(\sum_{i=1}^4 e_i^T(t) e_i(t) \right) \quad (18)$$

By evaluating the derivative of $V(t)$ along the trajectories of system (18), the following expression is obtained:

$$\begin{aligned} \dot{V}(t) &= \sum_{i=1}^4 e_i^T(t) \dot{e}_i(t) = \\ &= \sum_{i=1}^4 e_i^T(t) \left(-\lambda_1 e_i(t) - \lambda_2 \operatorname{sign}(e_i(t)) |e_i(t)|^{1+\gamma_1} - \lambda_3 \operatorname{sign}(e_i(t)) |e_i(t)|^{1-\gamma_1} - \right. \\ &\quad \left. - \lambda_4 \operatorname{sign}(e_i(t)) |e_i(t)|^{1+\gamma_1} \right) \leq \\ &\leq - \sum_{i=1}^4 e_i^T(t) \lambda_1 e_i(t) - \sum_{i=1}^4 e_i^T(t) \lambda_2 \operatorname{sign}(e_i(t)) |e_i(t)|^{1+\gamma_1} - \sum_{i=1}^4 e_i^T(t) \lambda_3 \operatorname{sign}(e_i(t)) |e_i(t)|^{1-\gamma_1} - \\ &\quad - \sum_{i=1}^4 e_i^T(t) \lambda_4 \operatorname{sign}(e_i(t)) |e_i(t)|^{1+\gamma_1} \leq \\ &\leq - \sum_{i=1}^4 e_i^T(t) \lambda_1 e_i(t) - \lambda_2 \sum_{i=1}^4 |e_i(t)|^{2+\gamma_1} - \lambda_3 \sum_{i=1}^4 |e_i(t)|^{2-\gamma_1} - \lambda_4 \sum_{i=1}^4 |e_i(t)|^{2+\gamma_1} = \\ &= - \sum_{i=1}^4 e_i^T(t) \lambda_1 e_i(t) - \lambda_2 \sum_{i=1}^4 (|e_i(t)|^2)^{\frac{2+\gamma_1}{2}} - \lambda_3 \sum_{i=1}^4 (|e_i(t)|^2)^{\frac{2-\gamma_1}{2}} - \lambda_4 \sum_{i=1}^4 (|e_i(t)|^2)^{\frac{2+\gamma_1}{2}}. \end{aligned} \quad (19)$$

From Lemma 1, the following result is obtained:

$$\begin{aligned} \dot{V}(t) &\leq -\lambda_1 V(t) - \lambda_2 4^{1-\frac{2+\gamma_1}{2}} \left(\sum_{i=1}^4 |e_i(t)|^2 \right)^{\frac{2+\gamma_1}{2}} - \lambda_3 \left(\sum_{i=1}^4 |e_i(t)|^2 \right)^{\frac{2-\gamma_1}{2}} - \\ &\quad - \lambda_4 4^{1-\frac{2+\gamma_1}{2}} \left(\sum_{i=1}^4 |e_i(t)|^2 \right)^{\frac{2+\gamma_1}{2}} = -\lambda_1 V(t) - \lambda_2 V(t)^{1+\frac{\gamma_1}{2}} - \lambda_3 V(t)^{1+\frac{\gamma_1}{2}} - \lambda_4 V(t)^{1+\frac{\gamma_1}{2}}. \end{aligned} \quad (20)$$

According to Theorem 1, the drive system (7) and the response system (8) are capable of achieving fixed-time synchronization when utilizing the controller (11). The proof has been finalized.

The synchronization performance between the driving system and the response system is demonstrated by the time responses of the corresponding state variables. After the proposed controllers are applied, the trajectories of the response system are observed to follow those of the driving system

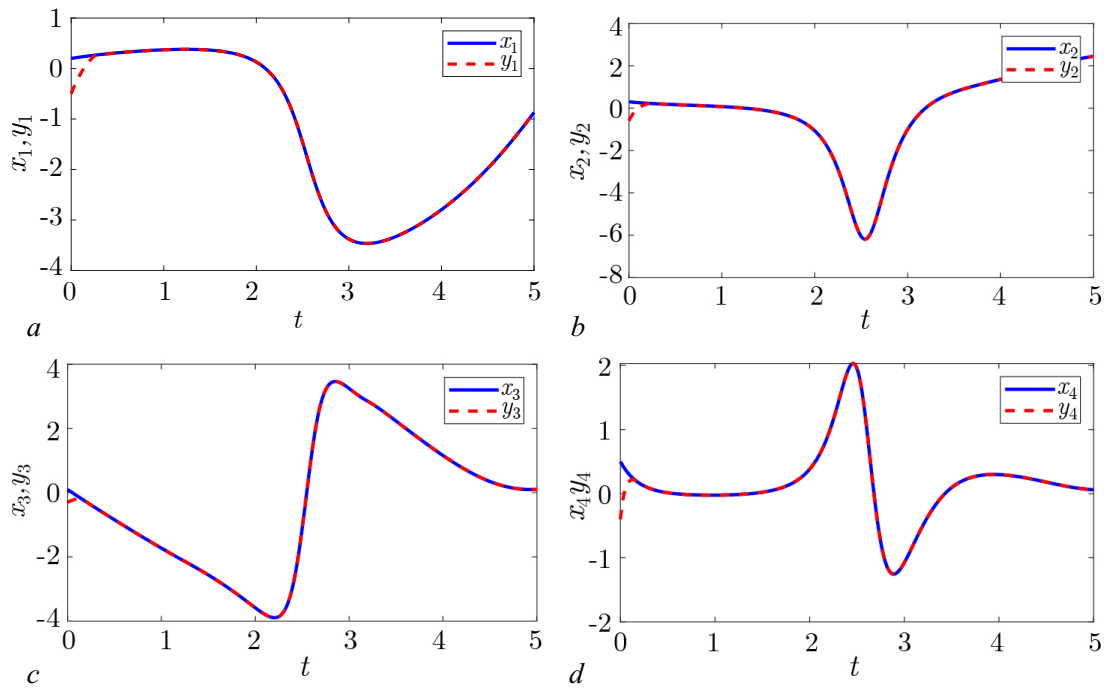


Fig. 6. The state variable synchronization diagram for chaotic systems with fixed time: $x_1 - y_1$ (a), $x_2 - y_2$ (b), $x_3 - y_3$ (c), $x_4 - y_4$ (d) (color online)

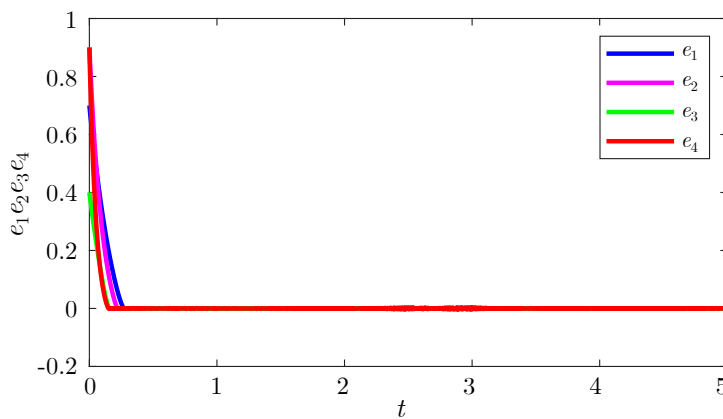


Fig. 7. The fixed-time synchronization error (color online)

accurately, which confirms the effectiveness of the developed control scheme, as illustrated in Fig. 6. In addition, the time evolution of the synchronization errors e_1 , e_2 , e_3 , and e_4 is presented. The rapid convergence of all error states toward zero further verifies that synchronization between the two systems is successfully achieved, as shown in Fig. 7.

4. Application to Networked Mobile Robots

Autonomous navigation of mobile robots in complex environments plays an important role in applications such as search-and-rescue, surveillance, and patrol missions. By incorporating the proposed four-dimensional chaotic dynamics into the robot control framework, unpredictable trajectories can be generated, thereby improving workspace exploration and motion flexibility.

The kinematic behavior of the mobile robot is described by the following nonholonomic model [42]:

$$\begin{cases} \dot{X}(t) = v(t) \cos \theta(t), \\ \dot{Y}(t) = v(t) \sin \theta(t), \\ \dot{\theta}(t) = \omega(t), \end{cases} \quad (21)$$

where $X(t)$ and $Y(t)$ denote the Cartesian coordinates of the robot, $\theta(t)$ represents its orientation angle, $v(t)$ is the linear velocity, and $\omega(t)$ is the angular velocity.

For a two-wheeled differential-drive mobile robot, the fractional-order kinematic model can be written as

$$\begin{cases} D^q X(t) = v(t) \cos \theta(t), \\ D^q Y(t) = v(t) \sin \theta(t), \\ D^q \theta(t) = \omega(t), \end{cases} \quad (22)$$

where D^q denotes the fractional derivative of order q . The linear and angular velocities are defined by

$$v(t) = \frac{v_R(t) + v_L(t)}{2}, \quad \omega(t) = \frac{v_R(t) - v_L(t)}{L},$$

with $v_R(t)$ and $v_L(t)$ representing the right and left wheel velocities, respectively, and L denoting the distance between the two wheels.

Within the master-slave synchronization framework, the states of the master robot are denoted by

$$x(t) = (x_1(t), x_2(t), x_3(t), x_4(t))^T,$$

whereas the states of the slave robot are denoted by

$$y(t) = (y_1(t), y_2(t), y_3(t), y_4(t))^T.$$

Accordingly, the linear and angular velocities of the master robot are expressed as

$$v_m(t) = \frac{x_1(t) + x_2(t)}{2}, \quad \omega_m(t) = \frac{x_1(t) - x_2(t)}{L},$$

while those of the slave robot are given by

$$v_s(t) = \frac{y_1(t) + y_2(t)}{2}, \quad \omega_s(t) = \frac{y_1(t) - y_2(t)}{L}.$$

Accordingly, a seven-dimensional coupled model is formulated to describe the motion of the master-slave mobile robotic system under the influence of the proposed chaotic dynamics, as follows:

$$\begin{cases} D^q y_1(t) = y_2(t) + u_1(t), \\ D^q y_2(t) = -y_3(t)y_2(t) - y_1(t) - a_1 y_4(t) + u_2(t), \\ D^q y_3(t) = a_2 y_2^4(t) - a_3 |y_2(t)| - a_5 + u_3(t), \\ D^q y_4(t) = -a_4 y_4(t) + y_2(t)y_3(t) + u_4(t), \\ D^q X(t) = v(t) \cos \theta(t), \\ D^q Y(t) = v(t) \sin \theta(t), \\ D^q \theta(t) = \omega(t). \end{cases} \quad (23)$$

For the numerical implementation, the parameters were selected as $a_1 = 0.5$, $a_2 = 0.9$, $a_3 = 1.5$, $a_4 = 5.5$, and $a_5 = 1.6$, while the control gains were chosen as $\lambda = [3, 2, 2.5, 1.5]$ and $\gamma = 0.8$, with wheel separation $L = 0.08$ m. Under these settings, accurate trajectory synchronization of the master–slave pair is achieved within a finite time. After synchronization is established, both robots are shown to follow closely matching chaotic trajectories inside the prescribed workspace, which confirms the effectiveness of the proposed control framework for coordinated motion generation and tracking, as illustrated in Fig. 8. These results demonstrate that the proposed formulation provides an effective link between the theoretical fractional-order chaotic model and its robotic implementation, while preserving coordinated motion and trajectory complexity.

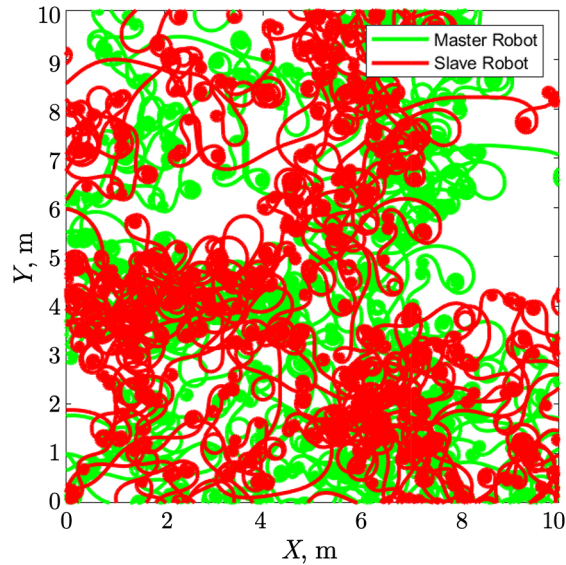


Fig. 8. Trajectory synchronization in X-Y plane. Green: master robot (x), red: slave robot (y). Inset shows convergence within initial 3 seconds (color online)

4.1. Multi-robot swarm synchronization. In the context of multi-robot systems, synchronization is crucial for ensuring coordinated actions and consistent behavior among multiple agents. Applications such as search-and-rescue missions, swarm robotics, and autonomous vehicle fleets require the ability to synchronize a large number of robots so that they operate cohesively in dynamic and complex environments [61, 62]. The master-slave synchronization approach presented in this work is designed to tackle this challenge, where one robot (the master) provides a reference trajectory, and the other robots (the slaves) follow this trajectory while maintaining synchronization across their states.

Synchronization of mobile robots with chaotic dynamics is particularly challenging due to the inherent unpredictability and nonlinear behavior of these systems. The introduction of chaotic dynamics allows for a more thorough exploration of the environment but requires careful coordination between robots to prevent divergence and instability. The proposed fixed-time synchronization framework provides a solution by ensuring that the synchronization is achieved in a finite, predictable amount of time, irrespective of initial conditions or system size [63]. The proposed fixed-time synchronization framework is extended to coordinate N robots in a swarm. Let the master system generate the reference chaotic trajectory $X_m(t)$, while N slave robots follow $X_s^i(t)$ ($i = 1, \dots, N$) with dynamics:

$$D^q X_s^i = f(X_s^i) + U_i + \sum_{j \in \mathcal{N}_i} \gamma_{ij} (X_s^j - X_s^i). \quad (24)$$

The distributed fixed-time controller is designed as:

$$U_i = -k_1 \text{sign}(e_i) |e_i|^\alpha - k_2 \text{sign}(e_i) |e_i|^\beta + \delta \begin{pmatrix} 0 \\ x_{3,m} \sin(x_{1,m}) \\ |x_{2,m}| \cos(x_{4,m}) \\ 0 \end{pmatrix}, \quad (25)$$

$$e_i = X_s^i - X_m, \quad \alpha = 1.8, \quad \beta = 0.6, \quad \delta = 0.2, \quad (26)$$

Theorem 4. The swarm system (24) under controller (26) achieves fixed-time synchronization if $k_1 > \|\nabla f(X_m)\|_\infty$ and $k_2 > \sqrt{N} \cdot d_{\max}$ where d_{\max} is maximum inter-robot distance. The settling time T_s satisfies:

$$T_s \leq \frac{1}{k_1(1-\beta)} \ln \left(1 + \frac{k_1 V(0)^{1-\beta}}{\eta} \right), \quad V = \frac{1}{2} \sum_{i=1}^N e_i^T e_i. \quad (27)$$

Proof 2. Consider the Lyapunov function $V = \frac{1}{2} \sum_{i=1}^N e_i^T e_i + \frac{1}{4} \sum_{i,j} \|X_s^i - X_s^j\|^2$. Taking fractional derivative:

$$\begin{aligned} D^q V &\leq \sum_{i=1}^N e_i^T D^q e_i + \frac{1}{2} \sum_{i,j} (X_s^i - X_s^j)^T (D^q X_s^i - D^q X_s^j) \\ &\leq -k_1 \sum_{i=1}^N |e_i|^{1+\beta} - k_2 \sum_{i=1}^N |e_i|^{1+\alpha} + \Phi, \end{aligned}$$

$$\Phi \leq \|\nabla f\|_\infty \|e_i\| - k_1 |e_i|^{1+\beta} \leq 0 \quad (\text{when } k_1 > \|\nabla f\|_\infty).$$

Thus $D^q V \leq -k_1 V^{(1+\beta)/2}$ proving fixed-time stability.

4.2. Discussion of synchronization and scalability results. The synchronization performance of the proposed control framework for a networked robotic system is illustrated through the time evolution of the state variable x_1 for the master and two representative slave units (Slave 1 and Slave 5).

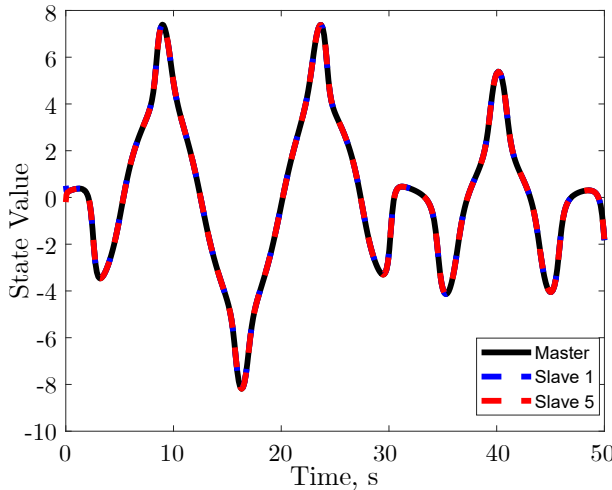


Fig. 9. Synchronization of state variable x_1 between Master, Slave 1, and Slave 5 (color online)

It can be observed that all trajectories converge rapidly toward the same reference trajectory, thereby demonstrating effective synchronization behavior. The very small phase lag and the close overlap among the curves further confirm that the designed control protocol ensures state convergence across all agents, as shown in Fig. 9. This level of synchronization is particularly notable given the nonlinear and potentially chaotic nature of the robot dynamics. The ability to achieve full-state synchronization (as seen in the virtually indistinguishable trajectories) validates the robustness of the control method against model complexities and disturbances. Moreover, this implies that the control input not only stabilizes each agent's dynamics but also enforces coherence across the entire multi-agent system.

4.3. Scalability analysis. To evaluate the scalability of the proposed synchronization algorithm, the average synchronization time was analyzed as the number of robots increased from 2 to 50. The results, presented in Fig. 10 and Table 1, were found to follow a highly efficient linear trend, with an approximate slope of 0.023 seconds per additional robot.

It is important to note that while Theorem 4 guarantees fixed-time convergence for the error dynamics of a single pair, the slight increase in synchronization time observed in the swarm simulation is attributed to the signal propagation delay inherent in the coupled network topology is seen in Eq. 24. Despite this, the near-linear behavior confirms that the computational and control overhead remains minimal, making the framework suitable for large-scale swarm deployments.

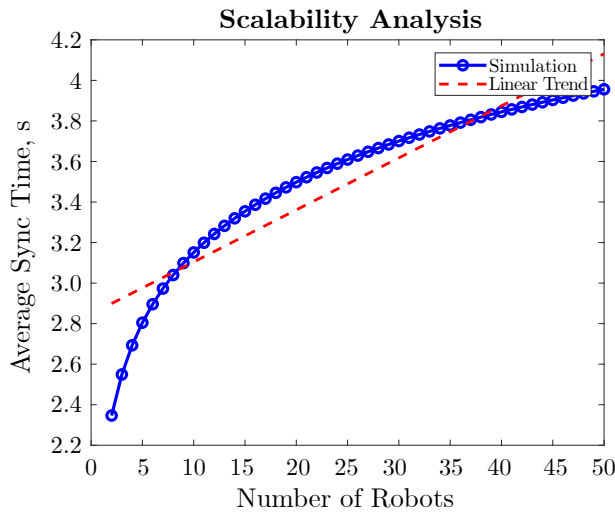


Fig. 10. Scalability analysis showing average synchronization time versus number of robots (color online)

Table 1. Average synchronization time as a function of number of robots

Number of Robots	Sync Time (s)
2	2.35
5	2.80
10	3.15
12	3.50
25	3.61
30	3.70
35	3.78
40	3.84
45	3.90
50	3.96

5. Discussion

The plot and data clearly indicate that synchronization time increases progressively with the number of robots. The linear regression trend exhibits a slope of approximately 0.023 seconds per robot. This result is highly efficient, indicating that as the system scales to 50 robots, the additional synchronization burden is minimal. The near-linear behavior indicates the algorithm’s strong scalability, with minimal performance degradation as system size increases.

The results illustrate an effective and scalable synchronization strategy for networked nonlinear robotic systems. High-precision synchronization at a low incremental cost per agent is infrequently documented in the literature. Many current methods experience exponential time growth or necessitate centralized computation, thereby restricting scalability.

A comparative analysis with recent and relevant literature is presented in Table 2 to contextualize the contributions of the proposed framework. A key distinguishing feature of this work is its proven scalability and guaranteed synchronization within a fixed time frame. This study presents robust simulation results for up to 50 robotic agents, demonstrating a near-linear and minimal increase in

Table 2. Comparison of robotic synchronization methods and contributions

Characteristic	This Work	Ref. [45]	Ref. [61]	Ref. [63]	Ref. [44]
Sync Method	Fixed-Time Sync	Generalized Sync	Fixed-Time Sync	General Sync	N/A (Single Robot)
Scalability	Excellent, tested to 50 robots	Obstacle-focused, less scalable	Theoretical focus	Multi-robot, no fixed-time focus	N/A (Single Robot)
Dynamics	4D Fractional-Order Chaos	Integer-Order Chaos	Chaotic Multi-Robot	Chaotic Dynamics	Integer-Order Chaos
Contribution	Scalable fixed-time sync framework	Obstacle avoidance with sync	Theoretical fixed-time sync	Multi-robot sync method	Single robot navigation

synchronization time, in contrast to other works that have examined fixed-time theory [61] or generalized synchronization for tasks such as obstacle avoidance [45]. This contrasts with methods based on single-robot navigation [44] or those that do not provide a fixed-time guarantee [63], which is essential for mission-critical applications that demand predictable convergence. The introduction of a novel 4D fractional-order chaotic system enhances dynamic complexity and modeling fidelity relative to the integer-order systems in the comparative studies. This analysis highlights that the framework offers a robust and efficient solution to the challenge of guaranteed-time synchronization in large-scale robotic swarms, addressing a significant gap in the current literature.

Conclusion

The present investigation has provided important insights into a previously unexplored four-dimensional chaotic system distinguished by the complete absence of equilibrium points. Through a detailed investigation of its integer-order and fractional-order forms, complex dynamical behaviors have been identified, including distinct chaotic attractors and transition mechanisms characterized by Lyapunov spectra and bifurcation diagrams. In particular, bistable behavior has been established through the coexistence of two attractors under the same parameter set and different initial conditions. To bridge theory and application, a fixed-time synchronization framework grounded in fractional stability theory has been developed, enabling coordinated dynamics between the fractional-order and integer-order representations. The synchronized system has been successfully employed for trajectory regulation in differential-drive mobile robots. Moreover, the proposed strategy has been shown to be fully distributed and capable of maintaining synchronization with a low and consistent temporal overhead. These features make the framework well suited for large-scale applications, including coordinated swarm robotics, decentralized sensor networks, and autonomous vehicles. Finally, the numerical results have validated both the synchronization performance and its usefulness in robotic navigation, thereby demonstrating the practical potential of the proposed method for cyber-physical systems subject to nonlinear dynamics and guaranteed-time convergence requirements.

References

1. Lorenz EN. Deterministic nonperiodic flow. *J. Atmos. Sci.* 1963;20(2):130–141. DOI: 10.1175/1520-0469(1963)020<0130:DNF>2.0.CO;2.
2. Wang X, Akgul A, Cicek S, Pham VT, Hoang DV. A chaotic system with two stable equilibrium points: dynamics, circuit realization and communication application. *Int. J. Bifurc. Chaos.* 2017;27(8):1750130. DOI: 10.1142/S0218127417501309.
3. Liao TL, Wan PY, Yan JJ. Design of synchronized large-scale chaos random number generators and its application to secure communication. *Appl. Sci.* 2019;9(1):185. DOI: 10.3390/app9010185.
4. Vaidyanathan S, Sambas A, Mamat M, Ws MS. A new three-dimensional chaotic system with a hidden attractor, circuit design and application in wireless mobile robot. *Arch. Control Sci.* 2017;27:541–554. DOI: 10.1515/acsc-2017-0032.
5. Yıldız BS, Kumar S, Pholdee N, Bureerat S, Sait SM, Yildiz AR. A new chaotic Lévy flight distribution optimization algorithm for solving constrained engineering problems. *Expert Syst.* 2022;39(8):e12992. DOI: 10.1111/exsy.12992.
6. Rössler OE. An equation for continuous chaos. *Phys. Lett. A* 1976;57(5):397–398. DOI: 10.1016/0375-9601(76)90101-8.
7. Chen F, Lin Y, Ren Z, Wang S. Uniform-in-time propagation of chaos for kinetic mean field Langevin dynamics. *Electron. J. Probab.* 2024;29(17):1–43. DOI: 10.1214/24-EJP1079.
8. Sprott JC. Some simple chaotic flows. *Phys. Rev. E.* 1994;50(2):R647–R650. DOI: 10.1103/PhysRevE.50.R647.

9. Wang N, Zhang G, Kuznetsov NV, Bao H. Hidden attractors and multistability in a modified Chua's circuit. *Commun. Nonlinear Sci. Numer. Simul.* 2021;92:105494. DOI: 10.1016/j.cnsns.2020.105494.
10. Dong C, Yang M, Jia L, Li Z. Dynamics investigation and chaos-based application of a novel no-equilibrium system with coexisting hidden attractors. *Physica A.* 2024;633:129391. DOI: 10.1016/j.physa.2023.129391.
11. Zaamoune F, Volos C. Sculpting chaos: Task-specific robotic control with a novel hopfield system and false attractors. *Symmetry.* 2025;17(12):2081. DOI: 10.3390/sym17122081.
12. Zaamoune F, Tinedert IE, Abro KA, Menacer T, Faizan M. A novel Chua circuit with hyperbolic tangent nonlinearity for brain-inspired dynamics and stable delta rhythm generation. *Int. J. Numer. Model.* 2026;39(1):e70141. DOI: 10.1002/jnm.70141.
13. Zaamoune F, Tinedert IE, Menacer T. Analysis of novel 3D chaotic system, hidden coexisting, adaptive control, offset boosting control, and circuit implementation. *Eur. J. Control.* 2025;8:101259. DOI: 10.1016/j.ejcon.2025.101259.
14. Zaamoune F, Tinedert IE, Menacer T, Wang N. Multistability and multi-spiral chaotic sea in a novel 3-D system with a line of equilibrium. *Phys. Scr.* 2025;100(3):035226. DOI: 10.1088/1402-4896/adb3d8
15. Zaamoune F, Tinedert IE, Abro KA, Faizan M. A novel approach to structured multistability in a 3D chaotic system: Implementation and circuit validation. *Int. J. Numer. Model.* 2024;38(6):e70123. DOI: 10.1002/jnm.70123.
16. Ahmad WM, Sprott JC. Chaos in fractional-order autonomous nonlinear systems. *Chaos Solitons and Fractals.* 2003;16(2):339–351. DOI: 10.1016/S0960-0779(02)00438-1.
17. Basti B, Hammami N, Berrabah I, Nouioua F, Djemiat R, Benhamidouche N. Stability analysis and existence of solutions for a modified SIRD model of COVID-19 with fractional derivatives. *Symmetry.* 2021;13(8):1431. DOI: 10.3390/sym13081431.
18. Bayani A, Jafari MA, Rajagopal K, Jiang H, Jafari S. A novel fractional-order chaotic system with specific topology: from proposing to FPGA implementation. *Eur. Phys. J. Spec. Top.* 2017;226:3729–3745. DOI: 10.1140/epjst/e2018-00031-y.
19. Zerimeche H, Houmor T, Berkane A. Combination synchronization of different dimensions fractional-order non-autonomous chaotic systems using scaling matrix. *Int. J. Dyn. Control.* 2021;9:788–796. DOI: 10.1007/s40435-020-00660-9.
20. Houmor T, Zerimeche H, Berkane A. Dynamical behaviors of fractional-order Selkov model and its discretization. *Nonlinear Dyn. Syst. Theory.* 2021;21:246–261.
21. Petráš I. A note on the fractional-order Chua's system. *Chaos Solitons and Fractals.* 2008;38(1):140–147. DOI: 10.1016/j.chaos.2006.10.054.
22. Lu JG, Chen G. A note on the fractional-order Chen system. *Chaos Solitons and Fractals* 2006;27(3):685–688. DOI: 10.1016/j.chaos.2005.04.037.
23. Luo C, Wang X. Chaos in the fractional-order complex Lorenz system and its synchronization. *Nonlinear Dyn.* 2013;71:241–257. DOI: 10.1007/s11071-012-0656-z.
24. Iskakova K, Alam MM, Ahmad S, Saifullah S, Akgül A, Yılmaz G. Dynamical study of a novel 4D hyperchaotic system: an integer and fractional order analysis. *Math. Comput. Simul.* 2023;208:219–245. DOI: 10.1016/j.matcom.2023.01.024.
25. Zhang X, Li Z. Hidden extreme multistability in a novel 4D fractional-order chaotic system. *Int. J. Non-Linear Mech.* 2019;111:14–27. DOI: 10.1016/j.ijnonlinmec.2019.01.009.
26. Wei D, Dong C. Dynamics, periodic orbits of a novel four-dimensional hyperchaotic system with hidden attractors. *Phys. Scr.* 2024;99(8):085251. DOI: 10.1088/1402-4896/ad61cc.
27. Yu F, Zhang S, Su D, Wu Y, Gracia YM, Yin H. Dynamic analysis and implementation of FPGA

- for a new 4D fractional-order memristive Hopfield neural network. *Fractal Fract.* 2025;9(2):115. DOI: 10.3390/fractalfract9020115.
28. Agrawal SK, Srivastava M, Das S. Synchronization of fractional order chaotic systems using active control method. *Chaos Solitons and Fractals.* 2012;45(6):737–752. DOI: 10.1016/j.chaos.2012.02.004.
 29. Pham VT, Ouannas A, Volos C, Kapitaniak T. A simple fractional-order chaotic system without equilibrium and its synchronization. *AEU-Int. J. Electron. Commun.* 2018;86:69–76. DOI: 10.1016/j.aeue.2018.01.023.
 30. Abro KA, Zaamoune F, Mahariq I, Faizan M. Thermal analysis of rotating fluid under fractal–fractional differential approach with G-Jitter effect: The dynamism of modulation. *Phys. Fluids.* 2025; 37:093124. DOI: 10.1063/5.0288914.
 31. Abro KA, Atangana A, Gómez-Aguilar JF. Optimal synchronization of fractal–fractional differentials on chaotic convection for Newtonian and non-Newtonian fluids. *Eur. Phys. J. Spec. Top.* 2023;232:2403–2414. DOI: 10.1140/epjs/s11734-023-00913-6.
 32. Aghababa MP. Finite-time chaos control and synchronization of fractional-order nonautonomous chaotic (hyperchaotic) systems using fractional nonsingular terminal sliding mode technique. *Nonlinear Dyn.* 2012;69:247–261. DOI: 10.1007/s11071-011-0261-6.
 33. Butusov D, Rybin V, Karimov A. Fast time-reversible synchronization of chaotic systems. *Phys. Rev. E.* 2025;111(1):014213. DOI: 10.1103/PhysRevE.111.014213.
 34. Li TZ, Tan XW, Wang Y, Wang QK. Analysis of stability and quasi-synchronization in fractional-order neural networks with mixed delays, uncertainties, and external disturbances. *Fractal Fract.* 2026;10(1):73. DOI: 10.3390/fractalfract10010073.
 35. Bendib I, Ouannas A, Dalah M. Mittag–Leffler synchronization of fractional-order reaction–diffusion systems. *Asian J. Control.* 2026;28:279–293. DOI: 10.1002/asjc.3702.
 36. He Y, Peng J, Zheng S. Fractional-order financial system and fixed-time synchronization. *Fractal Fract.* 2022;6(9):507. DOI: 10.3390/fractalfract6090507.
 37. Cheng Y, Yang W, Xu W, Zhong S. Impulsive effects on delayed fractional-order neural networks: sliding mode control-based fixed-time synchronization analysis. *Nonlinear Dyn.* 2025;113:16571–16592. DOI: 10.1007/s11071-025-10955-1.
 38. Sun Y, Liu Y, Liu L. Fixed-time synchronization for fractional-order cellular inertial fuzzy neural networks with mixed time-varying delays. *Fractal Fract.* 2024;8(2):97. DOI: 10.3390/fractalfract8020097.
 39. Danca MF, Kuznetsov N. Matlab code for Lyapunov exponents of fractional-order systems. *Int. J. Bifurc. Chaos.* 2018;28(5):1850067. DOI: 10.1142/S0218127418500670.
 40. Danca MF. Matlab code for Lyapunov exponents of fractional-order systems, part II: The noncommensurate case. *Int. J. Bifurc. Chaos.* 2021;31(12):2150187. DOI: 10.1142/S021812742150187X.
 41. Ding Y, Liu H. A new fixed-time stability criterion for fractional-order systems. *AIMS Math.* 2022;7(4):6173–6181. DOI: 10.3934/math.2022343.
 42. Nakamura Y, Sekiguchi A. The chaotic mobile robot. *IEEE Trans. Robot. Autom.* 2001;17(6):898–904. DOI: 10.1109/70.976022.
 43. Zang X, Iqbal S, Zhu Y, Liu X, Zhao J. Applications of chaotic dynamics in robotics. *Int. J. Adv. Robot. Syst.* 2016;13(2):60. DOI: 10.5772/62796.
 44. Nwachioma C, Pérez-Cruz JH. Analysis of a new chaotic system, electronic realization and use in navigation of differential drive mobile robot. *Chaos Solitons and Fractals.* 2021;144:110684. DOI: 10.1016/j.chaos.2021.110684.
 45. Marwan M, Li F, Ahmad S, Wang N. Mixed obstacle avoidance in mobile chaotic robots

- with directional keypads and its non-identical generalized synchronization. *Nonlinear Dyn.* 2025;113:2377–2390. DOI: 10.1007/s11071-024-10361-z.
46. Li Y, Li C, Yu W, Lei T, Li RYM. Symmetric pseudo-multi-scroll attractor and its application in mobile robot path planning. *Symmetry.* 2024;16(7):868. DOI: 10.3390/sym16070868.
 47. Abro KA, Atangana A, Gómez-Aguilar JF. Chaos control and characterization of brushless DC motor via integral and differential fractal-fractional techniques. *Int. J. Model. Simul.* 2023;43(4): 416–425. DOI: 10.1080/02286203.2022.2086743.
 48. Valencia-Ponce MA, González-Zapata AM, de la Fraga LG, Sanchez-Lopez C, Tlelo-Cuautle E. Integrated circuit design of fractional-order chaotic systems optimized by metaheuristics. *Electronics.* 2023;12(2):413. DOI: 10.3390/electronics12020413.
 49. Singh AP, Bingi K. Applications of fractional-order calculus in robotics. *Fractal Fract.* 2024;8(7): 403. DOI: 10.3390/fractalfract8070403.
 50. Kethiri MF, Charrouf O, Betka A, Tibermacine IE, Napoli C. Hybrid fuzzy-PSO based self-tuning fractional order PI controller for BLDC motors in electric vehicles: Comparative analysis and experimental validation. *J. Vib. Control.* 2025;10775463251374112. DOI: 10.1177/10775463251374112.
 51. Kethiri MF, Charrouf O, Betka A, Salman M, Boccaletti C. Minimizing power losses in BLDC motor drives through adaptive flux control: A real-time experimental study. *Actuators.* 2025;14(8):395. DOI: 10.3390/act14080395.
 52. Yurdem B, Aksu MF, Sagbas M. Microcontroller realization of a novel 4D hyperchaotic system and its autonomous mobile robot application. *Informacije MIDEM.* 2025;55(3):151–165. DOI: 10.1109/ISDFS58141.2023.10131716.
 53. Labbadi M, Boubaker S, Djemai M, Mekni SK, Bekrar A. Fixed-time fractional-order global sliding mode control for nonholonomic mobile robot systems under external disturbances. *Fractal Fract.* 2022;6(4):177. DOI: 10.3390/fractalfract6040177.
 54. Cui Y, Zheng Z. Novel fractional-order chaotic system applied to mobile robot path planning and chaotic path synchronization. *Symmetry.* 2025;17(3):350. DOI: 10.3390/sym17030350.
 55. Das S. *Functional Fractional Calculus for System Identification and Controls.* Berlin: Springer; 2007. 240 p. DOI: 10.1007/978-3-540-72703-3.
 56. Samko SG, Kilbas AA, Marichev OI. *Fractional Integrals and Derivatives: Theory and Applications.* Boca Raton: CRC Press; 1993. 1016 p.
 57. Benettin G, Galgani L, Giorgilli A, Strelcyn JM. Lyapunov characteristic exponents for smooth dynamical systems and for Hamiltonian systems; a method for computing all of them. Part 1: Theory. *Meccanica.* 1980;15:9–20. DOI: 10.1007/BF02128236.
 58. Diethelm K, Ford NJ, Freed AD. A predictor-corrector approach for the numerical solution of fractional differential equations. *Nonlinear Dyn.* 2002;29:3–22. DOI: 10.1023/A:1016592219341
 59. Hardy GH, Littlewood JE, Pólya G. *Inequalities.* Cambridge: Cambridge University Press; 1952. 324 p.
 60. Ouannas A, Abu-Saris R. A robust control method for Q - S synchronization between different dimensional integer-order and fractional-order chaotic systems. *J. Control Sci. Eng.* 2015;2015(4): 703753. DOI: 10.1155/2015/703753.
 61. Li S, Zhang S, He G, Jiang T. Discrete-time flocking control in multi-robot systems with random link failures. *IEEE Transactions on Vehicular Technology.* 2024;73(9):12290–12304. DOI: 10.1109/TVT.2024.3382617.
 62. Sun F, Li H, Zhu W, Kurths J. Fixed-time formation tracking for multiple nonholonomic wheeled mobile robots based on distributed observer. *Nonlinear Dynamics.* 2021;106:3331–3349. DOI: 10.1007/s11071-021-06946-7.
 63. Zhou L, Tokekar P. Multi-robot coordination and planning in uncertain and adversarial environments. *Current Robotics Reports.* 2021;2:147–157. DOI: 10.1007/s43154-021-00046-5.



Заамун Файза — профессор лаборатории прикладной математики математического факультета университета Мохамеда Хидера Бискры (Алжир). Phd в области математики (университет Бискры). Научные интересы: хаос, теория бифуркаций, системы с дробным хаосом, шифрование изображений, мобильные роботы и нейронные сети.

Алжир, 07000 Бискра, ВР 145 RP
Университет Мохамеда Хидера Бискры
E-mail: faiza.zaamoune@univ-biskra.dz
ORCID: 0000-0002-0099-4952

Зеримеш Хаджер — исследователь, специалист в области прикладной нелинейной динамики и теории дробного исчисления. Работает на факультете точных наук университета Константина 1 (Алжир).

Алжир, 25017 Константин, улица Айн-эль-Бей, 325
Университет братьев Ментури Константина 1
E-mail: hadjer.zerimeche@umc.edu.dz



Ибрахим Рабха Вазл — профессор научно-исследовательского центра университета Аль-Айен (Ирак). Phd в области сложных систем (2011, Центр моделирования и анализа данных в Национальном университете Малайзии). Имеет сертификат Google Data Analytics от Coursera (2022, США). Научные интересы: сложные системы, облачные системы, математическое моделирование, пересечение фракталов и дробное исчисление с приложениями в различных научных областях.

Ирак, Насирия, Thi Qar, Nile Street
Университет Аль-Айен
E-mail: rabhaibrahim@yahoo.com
ORCID: 0000-0001-9341-025X



Каримов Артур Искандарович — кандидат технических наук (2017, СПбГЭТУ «ЛЭТИ»), магистр английского языка (2014, СПбГЭТУ «ЛЭТИ»). Доцент кафедры автоматизированного проектирования Санкт-Петербургского государственного электротехнического университета «ЛЭТИ». Научные интересы: робототехника, искусственный интеллект, идентификация систем и теория хаоса.

Россия, 197022 Санкт-Петербург, ул. Профессора Попова, 5Ф
Санкт-Петербургский государственный электротехнический университет «ЛЭТИ»
E-mail: aikarimov@etu.ru
ORCID: 0000-0002-2591-0962
AuthorID (eLibrary.Ru): 767425